ELSEVIER

Precision Engineering 24 (2000) 99–118

PRECISION ENGINEERING

Dynamic evaluation of spatial CNC contouring accuracy

Tony Schmitz[a,†], John Ziegert[b,*]

[a]*Automated Production Technology Division, Manufacturing Engineering Laboratory, National Institute of Standards and Technology, Gaithersburg, Maryland*

[b]*Department of Mechanical Engineering, University of Florida, Gainesville, Florida*

Received 3 June 1999; received in revised form 10 September 1999; accepted 10 September 1999

Abstract

An instrument capable of measuring arbitrary, dynamic CNC tool paths through three-dimensional space with micrometer-level accuracy is developed and tested. The instrument uses three Laser Ball Bars simultaneously (i.e., simultaneous trilateration) to allow for dynamic path measurements. The design of the instrument is described. The performance is verified by static repeatability testing, comparison with an independent measurement system, and comparison with the dimensions of machined parts. The instrument is demonstrated to be capable of measurement of arbitrary three dimensional tool paths with near micron level accuracy. Published by Elsevier Science Inc.

Keywords: Spatial metrology; Dynamic path measurement; Contouring errors; Laser ball bar

1. Introduction

In computer numerical control (CNC) machining, the desired spatial trajectory of the cutting tool is ideally defined by the part program. The purpose of the part program is to place the tool tip at particular coordinates relative to the part at every instant in time, leaving behind newly created surfaces that form a workpiece of the proper dimensions. Errors in the final dimensions of the machined part are determined by the accuracy with which the commanded tool trajectory is followed, combined with any deflections of the tool, part, or machine caused by the cutting forces. The accuracy of the tool trajectory is dependent on the static machine geometry, the thermal state of the machine, and dynamic errors of the machine/control system. Using current technology, it is possible to measure the quasistatic geometric errors of a machine tool and their thermally induced deviations. With these data, we can construct a thermal/geometric error model of the machine that predicts the static tool point positioning error anywhere in the workspace and at any thermal state [1]. This machine error model can be used to predict tool position errors at discrete points along arbitrary CNC paths and predict the dimensional errors of a machined part that are caused by the imperfect machine geometry. It is also possible to machine parts using the same CNC part paths and then measure the actual dimensions of the resulting parts. Comparisons of the predicted and actual part dimensions show that the thermal/geometric error model obtained from static measurements is capable of predicting some, but not all, of the resulting part dimensional errors [1–3]. To improve the accuracy of models seeking to predict part dimensions, it is necessary to extend these models to include trajectory following errors related to the controller, as well as errors induced by the forces generated in the cutting process.

The purpose of this text is to describe and demonstrate the use of an instrument capable of measuring arbitrary, dynamic tool paths through three-dimensional (3-D) space with micrometer-level accuracy. The results of these dynamic path measurements can ultimately be used in two ways. First, differences between the measured dynamic path and the path predicted by the static thermal/geometric error model must be attributable to dynamic effects inherent in the control system of the machine. The dynamic errors can then be separated from the thermal/geometric errors and used to evaluate, model, and optimize the contouring performance of NC systems. Second, differences between the measured dynamic path of the tool (with no cutting) and the final part dimensions must be caused by forces generated in the cutting process. These discrepancies between part di-

* Corresponding author. Tel.: +352-392-0828; fax: +352-392-1071.
E-mail address: johnz@ufl.edu (J. Ziegert).

† Research completed at the University of Florida.

0141-6359/00/$ – see front matter Published by Elsevier Science Inc.
PII: S0141-6359(99)00034-3

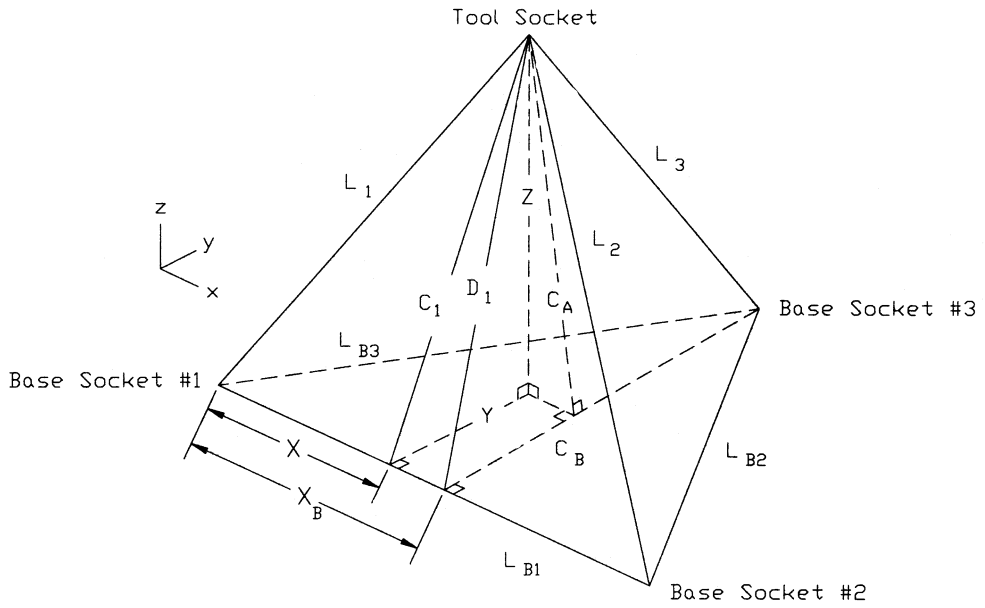

Fig. 1. Simultaneous trilateration.

mensions and dynamic path errors may then be used to understand and model the cutting process dynamics. Therefore, we believe that the ability to perform dynamic spatial CNC tool path measurements is a vital step toward the ability to understand and correctly model all sources that lead to part dimensional errors, and eventually the ability to predict final part dimensions (for a given CNC part program) based on a set of preprocess measurements performed on the machine.

The instrument described here for the measurement of dynamic spatial paths is based on the laser ball bar (LBB), developed by Ziegert and Mize [4,5]. The laser ball bar uses sequential trilateration to measure the static spatial coordinates of the tool at arbitrary points throughout the work volume of a CNC machine tool. The instrument described here uses three LBBs simultaneously (i.e., simultaneous trilateration) to allow for dynamic path measurements. The design and testing of this instrument have been described previously [6]. However, as a convenience to the reader, we include a brief description here, along with some typical test results.

2. Simultaneous trilateration

In this research, simultaneous trilateration was implemented to calculate the spatial coordinates of points along arbitrary CNC contours. In trilateration, a tetrahedron is formed by placing four sockets in a machine tool's work volume. Three of the sockets are rigidly fixed to the machine table. These sockets are referred to as the base sockets. The fourth socket (the tool socket) is mounted in the machine spindle at the tool point and traces the path followed by the cutting tool during the machine tool's dynamic contouring motions. If the lengths of the six edges of the tetrahedron are known, the spatial coordinates of the tool socket (in the local trilateration coordinate system) may be calculated (see Fig. 1).

The lengths between the three base sockets (L_{B1}, L_{B2}, L_{B3}) shown in Fig. 1 are measured once and are assumed to remain constant during the motion of the tool socket. The three base-to-tool socket lengths (denoted L_1, L_2, L_3 in Fig. 1) are measured simultaneously at regular time intervals by three separate measurement transducers during the execution of a given CNC part program. Because all three base-to-tool socket lengths are obtained at (ideally) the same instant in time for each measurement point, this method is referred to as simultaneous trilateration.

Previous research has focused on sequential trilateration [2,5,7]. In sequential trilateration, only one transducer is required, and the part program is executed three times with one base-to-tool socket length obtained during each run. In practical applications, this method is limited to static (geometric) measurements; whereas, simultaneous trilateration is well suited to dynamic measurements.

Simultaneous trilateration requires that each of the three transducer axes meet at a single point (at the tetrahedron vertex in Fig. 1). Fig. 2 shows a closer view of the spherical joint (located at the tool socket) that supports the three measurement transducers during simultaneous trilateration. As the tool socket follows the machine contours, the spatial coordinates of the tool point vary. Because the base sockets are fixed in space, the tool point motion causes the lengths of the individual transducers to change as well as the relative angles between them. This motion requires a joint that provides three independent angular degrees of freedom for

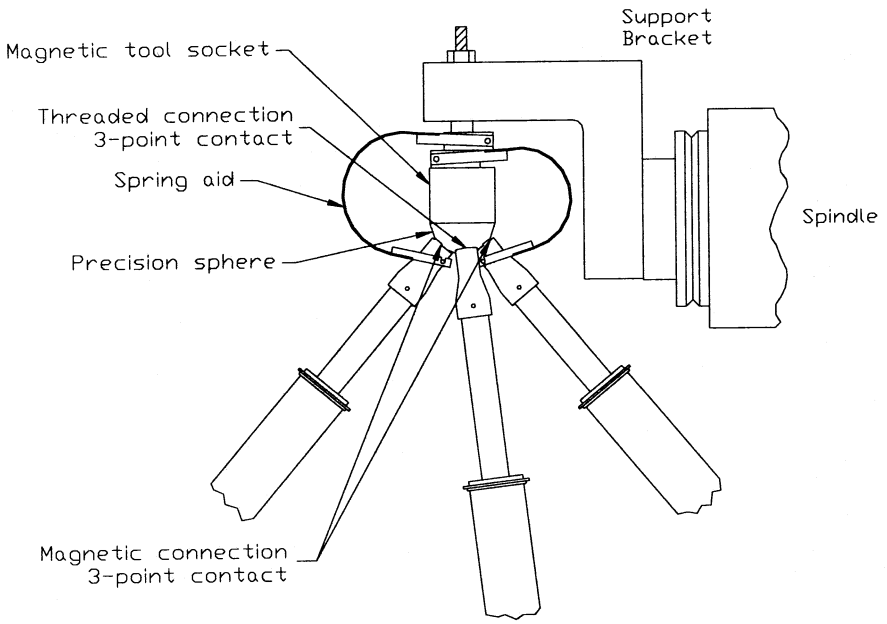

Fig. 2. Spherical joint.

each transducer, while prohibiting relative axial translations between the endpoints of each of the three transducer (e.g., a spherical joint).

For this research, the tool socket joint was attached to a machine spindle at a typical tool offset by a stiff bracket mounted on a standard 50-taper tool holder. The spindle was then locked against possible rotation during the measurements. One of the transducers was attached to a Grade 5, 38.1-mm diameter precision tool sphere by a removable threaded stud and three-point contact, and the other two were held in place by neodymium magnets mounted in three-point contact sockets, with additional support provided by spring aid assemblies. The three-point kinematic mounts were necessary to ensure that the location of the intersection of the three transducer axes (ideally at the sphere geometric center) did not change as the angular orientation varied during path motion. The spring aid assemblies were developed to make sure that the corresponding sockets slid smoothly over the surface of the sphere, rather than tip off it, under high accelerations.

As noted, the transducer used to measure the six sides of the trilateration tetrahedron in this research is the laser ball bar (LBB). The LBB is a precision linear displacement measuring device. It consists of a two-stage telescoping tube with a precision sphere mounted at each end (see Fig. 3). A heterodyne displacement measuring interferometer is aligned inside the tubes and measures the relative displacement between the two sphere centers. The heterodyne (two frequency) laser light is carried from a remote He–Ne, frequency-stabilized laser head to the Michelson-type interferometer by a single-mode,

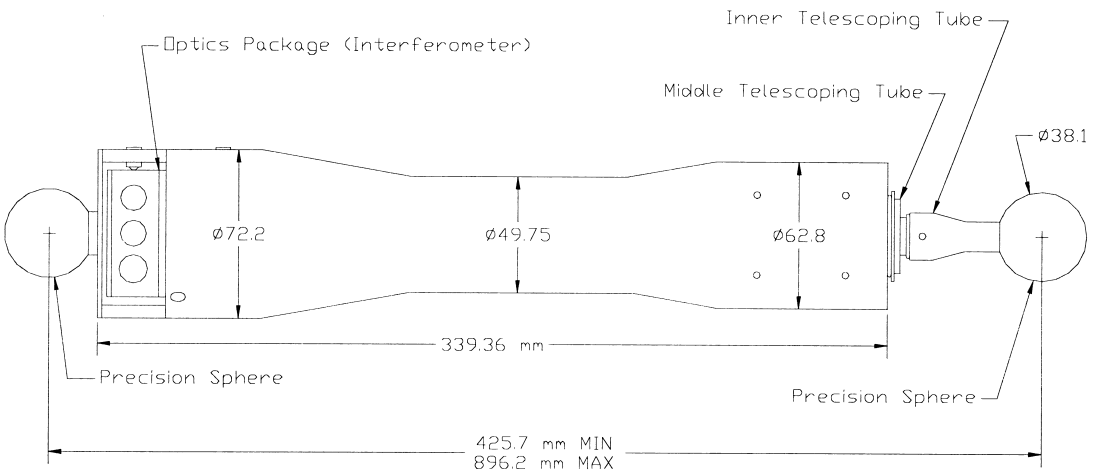

Fig. 3. Laser ball bar.

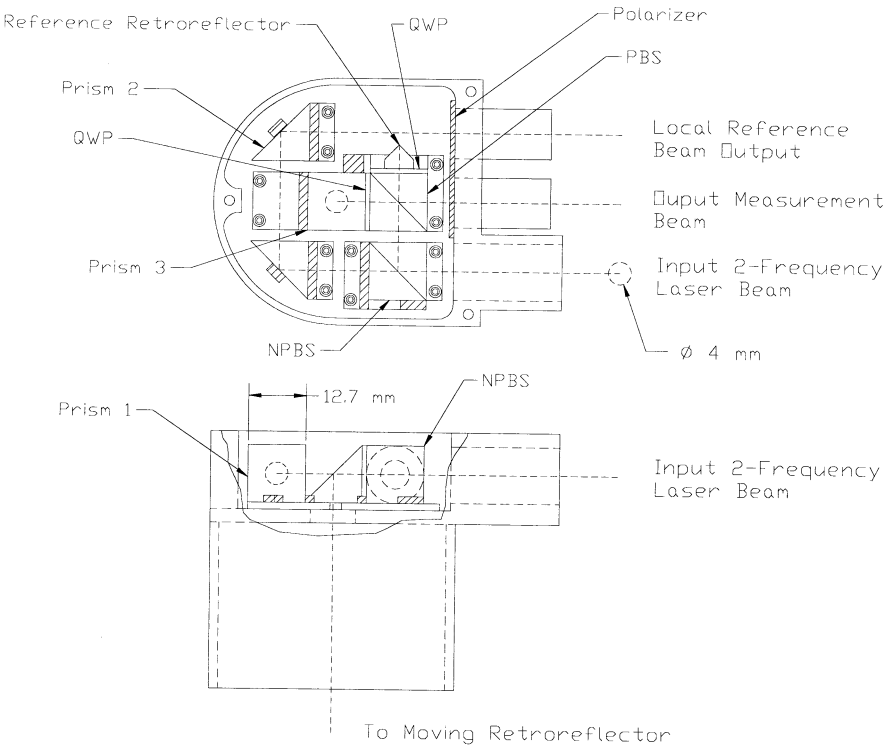

Fig. 4. Optics package.

polarization-maintaining (SMPM) fiber. The initial orthogonal polarization of the two light frequencies (leaving the laser head) are essentially maintained as they pass through the fiber by an internal birefringence (index of refraction dependent on direction of propagation).

At the LBB, a local phase reference is generated to eliminate the inherent cable-induced phase shifts between the two light frequencies (in the fiber optic cable) attributable to mechanical or thermal deformations of the SMPM fiber. The local phase reference signal and the measurement signal from the interferometer are carried to the phase-measuring electronics via two multimode (MM) optical fibers. The final linear displacement is calculated from the phase difference between the measurement signal (representing the actual LBB displacement combined with the SMPM errors) and local phase reference signal (containing only the SMPM fiber-induced displacement errors). The LBB has been shown to be accurate to submicrometer levels during static measurements [8].

Fig. 4 shows the optics package located in each LBB. The 4-mm diameter input laser beam is shown at the lower right-hand side of the top view. This beam is first split into two components by the nonpolarization beam splitter (NPBS). The transmitted portion (approximately 15%) is routed via prisms 1 and 2 to a polarizer (i.e., polarizing filter) oriented at 45° to the two orthogonal polarizations in the heterodyne signal, causing the two frequency components to interfere. The interference signal is carried to a photodetector by a MM fiber where the electronic local phase reference signal is generated. Any variation of the phase (i.e., measured displacement) in this reference signal attributable to fiber optic-induced phase shifts will be present in both the measurement and reference signals and will, therefore, be removed from the final displacement measurement.

The portion of the light initially reflected at the NPBS travels to a Michelson-type interferometer (composed of a polarization beam splitter, two retroreflectors, and two quarter wave plates) and is directed along the centerline of the telescoping tubes. The phase of the interfered measurement signal from the interferometer is compared to the phase of the local reference signal to obtain the final measurement signal, which represents the actual displacement of the moving retroreflector.

Because the linear displacement interferometer is only able to measure changes in displacement and not absolute distance, each LBB must be initialized before use to determine the sphere-center to sphere-center length. The initialization procedure is composed of three steps (see Fig. 5). First, the LBB is placed between sockets 1 and 2 of the initialization fixture, and the displacement counter is zeroed. Next, the LBB is extended from socket 2 to 3, and the displacement is recorded. This displacement is the distance between sockets 2 and 3. Finally, the LBB is placed between sockets 2 and 3, and the length of the LBB is initialized to the previously recorded displacement. The entire procedure takes less than 1 minute, thus minimizing any length changes in the initialization fixture caused by temperature fluctuations. Because the initialization length is measured directly during the initial-

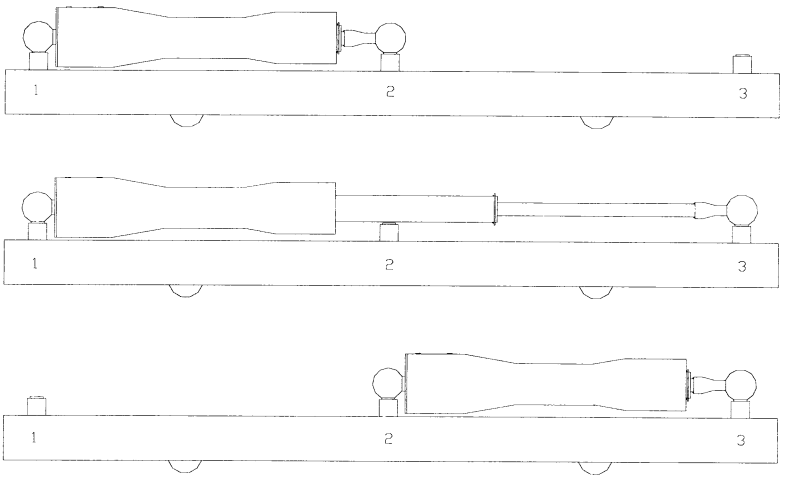

Fig. 5. Initialization procedure.

ization procedure, the initialization fixture need not be calibrated externally, and the LBB is essentially a "self-proving" device.

3. STLBB performance verification

Evaluation of the measurement performance of the Simultaneous Trilateration Laser Ball Bar (STLBB) system consisted of three activities: (1) comparison of STLBB results to those of an independent dynamic measuring device; (2) evaluation of the dynamic repeatability of the measurement system; and (3) static repeatability performance testing. The setup for the STLBB system measurements is shown in Fig. 6.

4. 2-D STLBB comparison

One method of testing the performance of a new measuring instrument is to compare its output to that of another instrument performing the same measurement. The ideal comparison device in this case should be capable of the measurement of the same 3-D dynamic contours as the STLBB system to the same (approximately $\pm$ 1 μm) or significantly better levels of accuracy. However, the closest match to this 3-D dynamic requirement was provided by an optical grid encoder, which is capable of 2-D dynamic measurements. The grid encoder used in this research was provided by the Heidenhain Corporation.

The Heidenhain KGM 101 Grid Encoder is composed of a grid plate (140-mm diameter) with a 2-D, waffle-type grating of closely spaced lines (4 μm signal period) and a

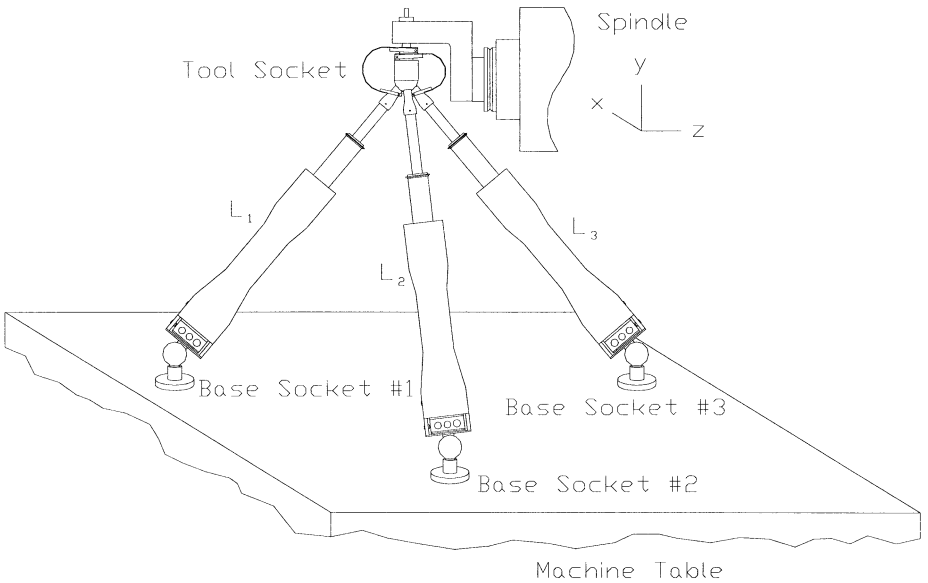

Fig. 6. STLBB system.

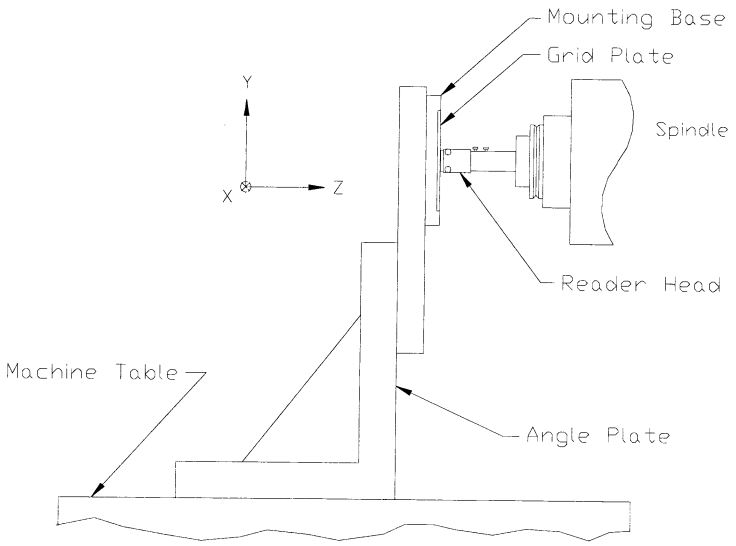

Fig. 7. Heidenhain setup.

noncontact scanning head that can measure translations in two directions. The optical grid plate is attached to an aluminum mounting base. This base is mounted in the plane to be measured (on an X–Y table, for example), and the scanning head is fixed perpendicular to the plate (e.g., on the Z-axis attached to the spindle). This system measures the relative planar motion between the grid and read head for any curvilinear path in the plane of the mounting base with a resolution of 4 nm and accuracy of ± 2 μm. The recorded motions allow the user to observe the dynamic effects of the machine tool's performance on 2-D CNC paths.

For this comparison, both instruments were configured to measure the same planar CNC paths. Fig. 7 shows the Heidenhain setup used for the 2-D measurements. Note that the measurement point is on the spindle centerline with the same Z-direction offset for both experimental setups. Therefore, geometric error variations within the work volume will not introduce a relative difference between the measurements (attributable to an Abbe offset). In addition, the CNC programs for both the STLBB and Heidenhain tests were executed from the same starting coordinates, so, again, any geometric variations within the machine tool's work volume would be minimized. Finally, the part programs were run in the same order from a cold machine state to minimize thermal deviations in the machine tool between the two sets of tests.

Several planar contours were selected to be measured with both measurement systems. These contours and their dimensions are summarized in Fig. 8. Although the measured paths were all confined to a single plane, the results were adequate to verify the spatial measurement performance of the STLBB based on the following argument.

1. The STLBB system requires no special alignment of its axes (by base socket placement) with the machine tool's coordinate system, and, in general, they are not aligned.
2. Although the commanded path is in two dimensions with respect to the machine tool, the spatial coordinates of this path lie in three dimensions in the STLBB system. (The trilateration coordinates are then transformed in the machine's coordinate system using a rotation matrix obtained by an independent LBB measurement to give the final 2-D results in machine coordinates.)
3. All of the measured contours require extension and/or contraction in length of all three individual LBBs, rotations of the LBBs within their respective sockets (change in angular orientation), or both.

Therefore, although all points on the commanded paths lie in a single plane, this plane is oriented arbitrarily to the STLBB system, and the coordinates of the measured points vary in all three coordinates in the STLBB system. For these paths, the types and ranges of required motions of the individual LBBs are identical to those required for a general 3-D path.

Comparisons between the Heidenhain and STLBB measurements are now presented. Three of the six verification contours (angle, step, sultan, square, triangle, and circle) are considered separately in the following paragraphs. All paths were executed at constant commanded accelerations (i.e., trapezoidal velocity profiles) of 0.98 to 4.91 m/s^2, with feedrates ranging from 889 to 1778 mm/min (35 to 70 inches per minute). In addition, a small motion in the positive X- and Y-directions was commanded before the execution of each CNC contour to minimize the effects of possible reversal errors in each axis. Both instruments were sampled at a nominal frequency of 1 kHz, which provided (minimum) spatial sampling rates of roughly 15 to 30 μm/sample at maximum steady-state velocity.

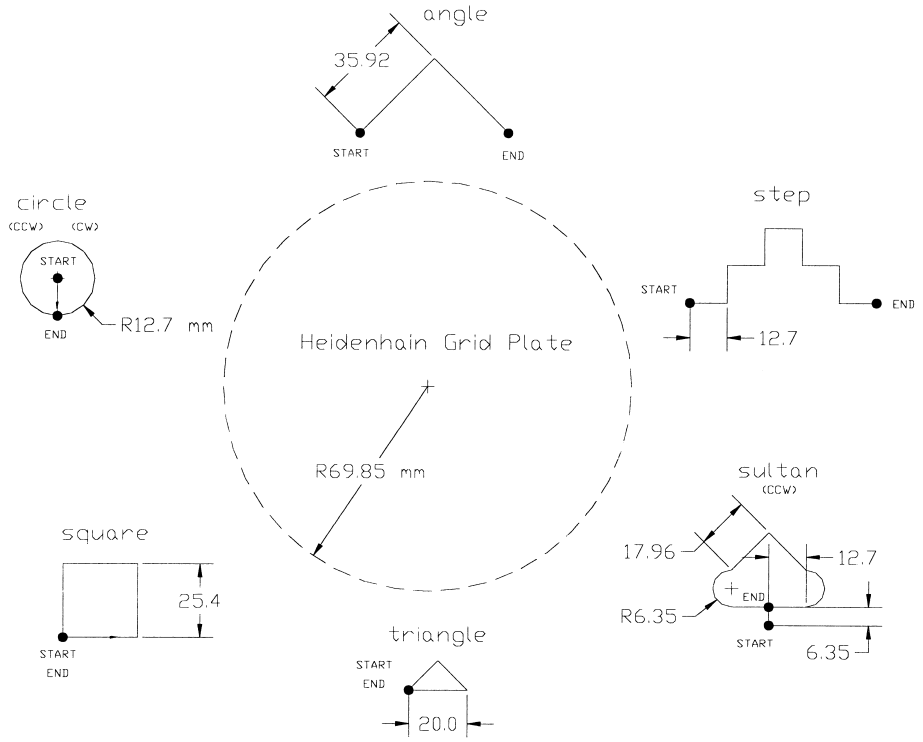

Fig. 8. Verification contours.

4.1. Angle path

The angle path includes motions in the X–Y plane that require linear interpolation in the two axes simultaneously. Fig. 9 shows a comparison between the Heidenhain grid plate and STLBB measurements for a feed of 889 mm/min and an acceleration of 0.98 m/s^2. *Only the cornering portion of the path is shown* to enhance the viewing resolution. Fig. 10 exhibits the two measurements for a feed of 1778 mm/min and an acceleration of 4.91 m/s^2.

This path aids in the tuning of the servomotors on machine tools. The measured response can be used to set the individual axis gains. If both axes have the same servo loop gain, then the steady-state servo lag for each axis (which is proportional to the axis velocity) will combine to create an actual tool path that lies along the same line as the commanded path, but lags the commanded position. For the

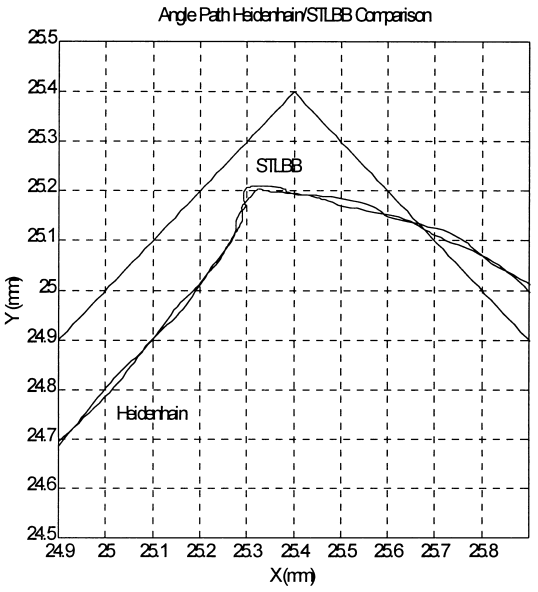

Fig. 9. Angle path comparison (889 mm/min, 0.98 m/s^2).

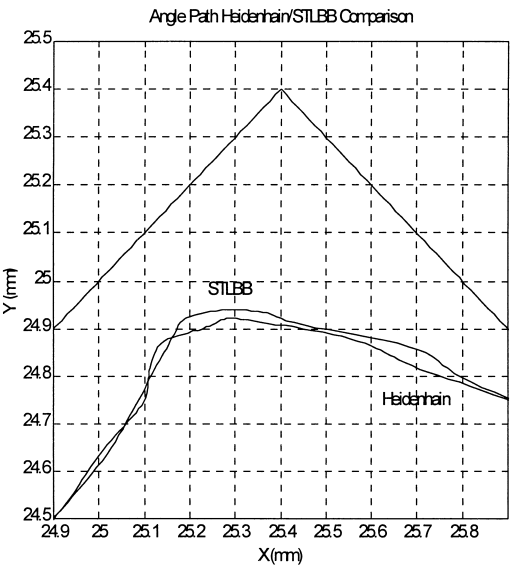

Fig. 10. Angle path comparison (1778 mm/min, 4.91 m/s^2).

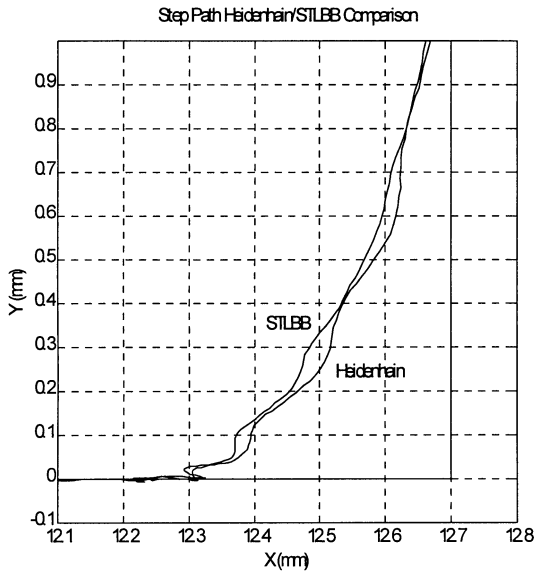

Fig. 11. Step path comparison (1778 mm/min, 0.98 m/s^2).

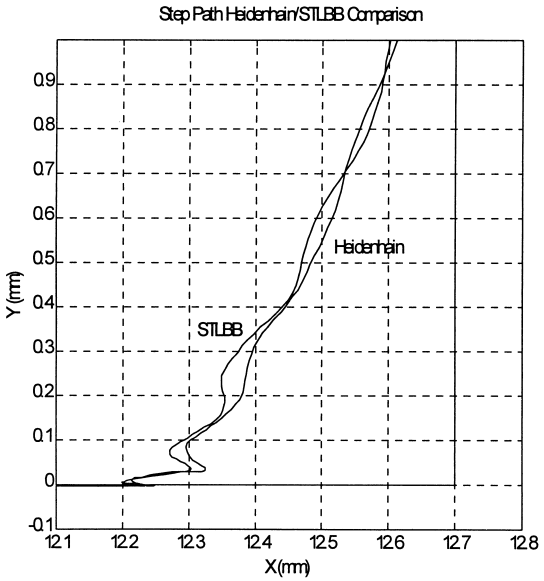

Fig. 12. Step path comparison (1778 mm/min, 4.91 m/s^2).

machine tool used in this research, however, a difference in the gain between the X- and Y-axes caused two different steady-state lag errors. Therefore, the actual contour is spatially offset from the commanded contour during constant velocity motion. Because this error is proportional to the commanded feed rate, the offset is seen to be approximately twice as large in Fig. 10 as in Fig. 9.

4.2. Step path

The step path includes linear interpolation in the X- and Y-axes individually and sharp corners with both positive and negative Y-direction motions. Consequently, this path can also be used to set the individual axis gains during tuning. Fig. 11 shows a comparison between the Heidenhain and STLBB measurements for the first cornering motion (+X to +Y) at a feed rate of 1778 mm/min and an acceleration of 0.98 m/s^2. Fig. 12 displays the same contour section at a feed of 1778 mm/min and 4.91 m/s^2 acceleration. Because of the low axis gain settings in this machine tool and the inherent velocity lag (i.e., commands are executed with some delay), there is a large undershoot seen in the cornering motion of both paths. In addition, an overshoot/corrective action controller effect is identified with both measurement systems in Fig. 12.

4.3. Circle path

Both counterclockwise and clockwise circle paths were also measured using the two measurement systems. The circle path is a historically popular dynamic evaluation contour, because its measurement can also be completed with the telescoping magnetic ball bar and/or disk check [9–12]. Figs. 13 and 14 display measurement results for clockwise and counterclockwise motions, respectively, with a commanded velocity of 1778 mm/min. The radial deviations of the measured path from the commanded have been amplified by a factor of five in both cases. Fig. 13 shows an elliptical distortion of the path with the major axis of the ellipse rotated 45° counterclockwise from the positive Y-axis. Fig. 14 exhibits the same elliptical distortion, but the major axis is now oriented at 135°. This directional-dependent, elliptical distortion of the circular paths was caused by the previously mentioned gain mismatch between the X- and Y-axes.

5. Dynamic repeatability

The good agreement between the optical grid plate and STLBB results at all feeds and accelerations served to verify

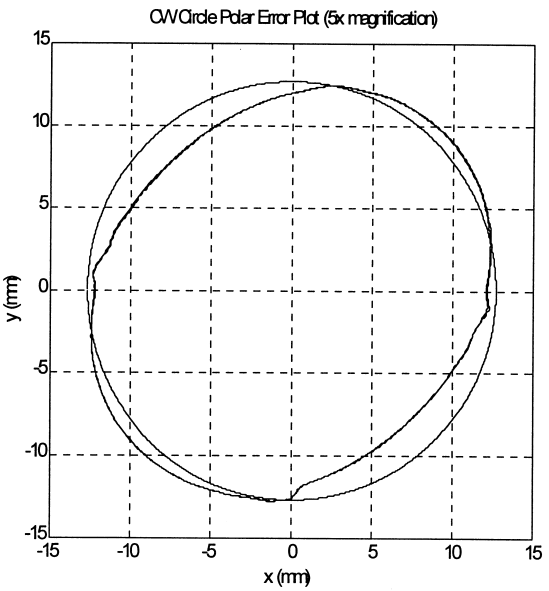

Fig. 13. Clockwise circle path comparison (1778 mm/min).

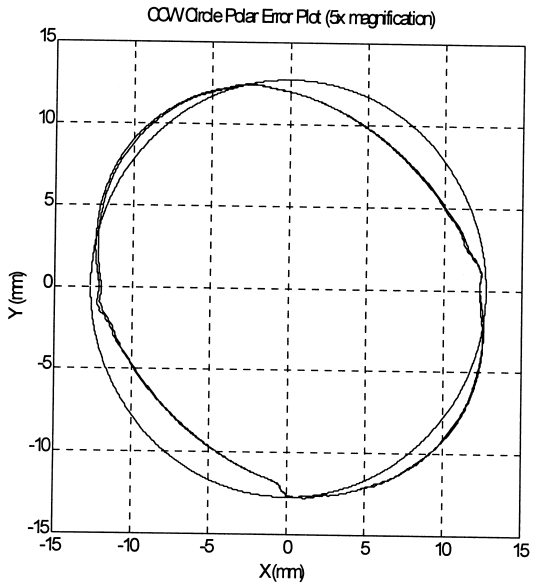

Fig. 14. Counter-clockwise circle path comparison (1778 mm/min).

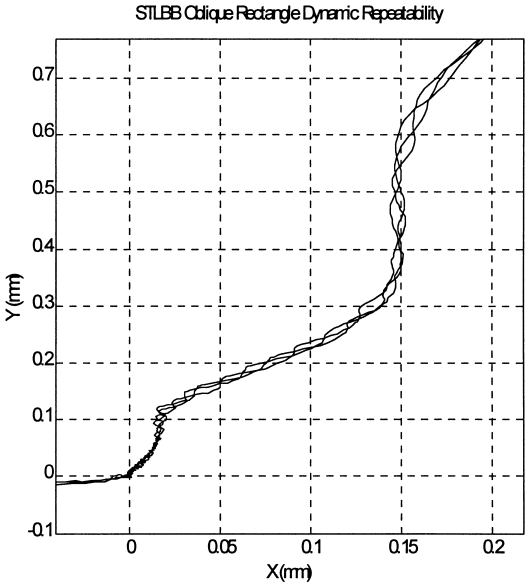

Fig. 16. STLBB dynamic repeatability test.

the usefulness of the STLBB as a dynamic measuring device. However, the measurement results did not provide the expected micrometer-level reproduction between the two measurement sets. Therefore, the dynamic repeatability of both measurement systems was evaluated. Fig. 15 shows three back-to-back dynamic path measurements using the Heidenhain grid plate. It can be seen that there is approximately a 20 μm error band that is necessary to contain the separate measurements. Similarly, three consecutive contours measured with the STLBB are shown in Fig. 16. In this case, a roughly 15 μm error band is recognized. Because the grid plate is a noncontact device, it cannot affect the machine tool's dynamic performance. Therefore, the dynamic contouring nonrepeatability of the measured motions are attributable to the dynamic nonrepeatability of the machine tool itself (the only machine available for this study) and not inherent in the measurement systems. The machine tool dynamic nonrepeatability, therefore, serves as a lower bound on the accuracy of the measurement comparison.

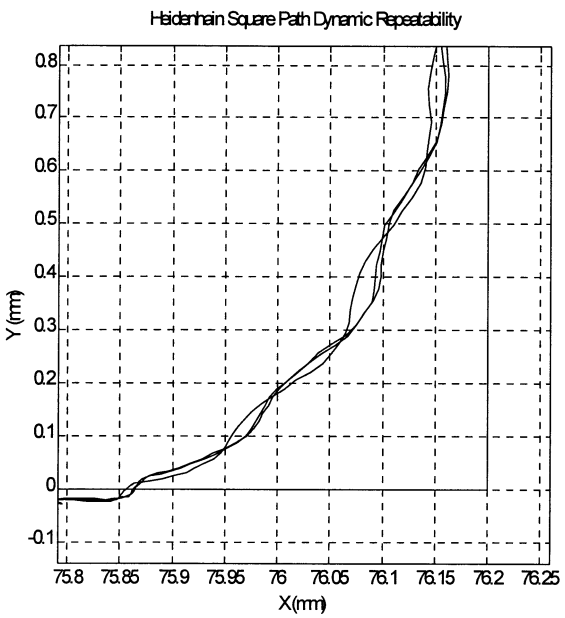

Fig. 15. Heidenhain dynamic repeatability test.

6. Static repeatability

The static measurement repeatability of the STLBB was evaluated using a capacitance probe. The capacitance probe setup is shown in Fig. 17. For these tests, the machine tool controller was programmed to move 6.35 mm in the +Y-direction, pause, and then return to the initial position. Twenty-five repetitions were completed using both the capacitance probe and STLBB setups, and the starting and ending positions were compared. At a feed of 889 mm/min, a maximum difference between return positions of 0.9 μm was found for the capacitance probe and a maximum difference of 1.3 μm for the STLBB. At 1778 mm/min, the maximum difference was 1.1 μm for the capacitance probe, and the STLBB maximum difference was 0.8 μm. These similar results suggest good static measurement repeatability for the STLBB measurement system.

7. Three-dimensional contour measurement results

To demonstrate the versatility of the STLBB system for 3-D dynamic path measurements, four different paths, combining multiaxis linear and circular interpolation, were chosen: corkscrew, hemisphere, oblique circle, and oblique rect-

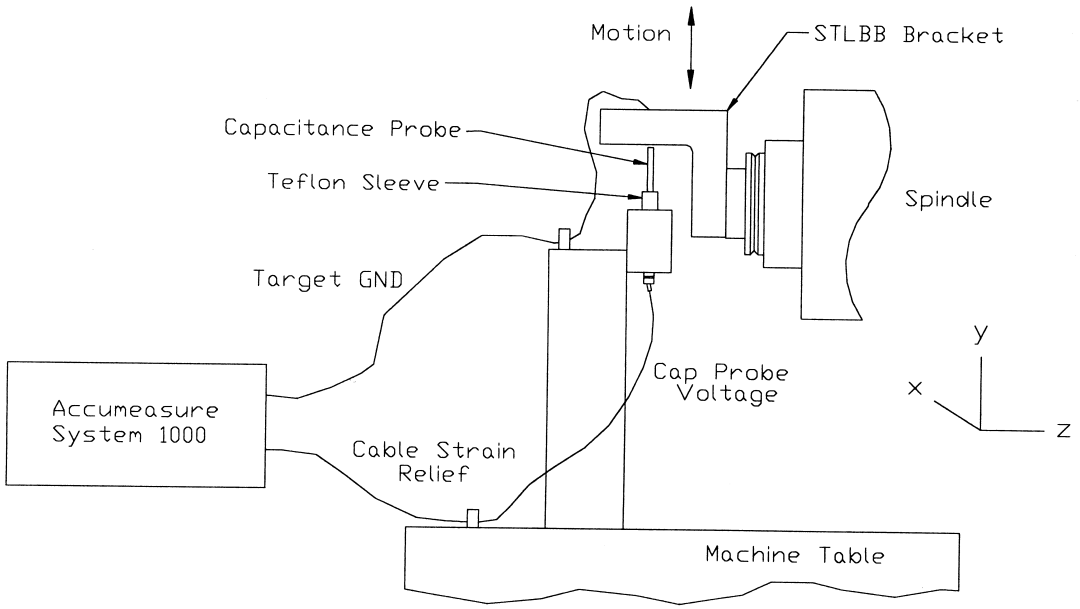

Fig. 17. Capacitance probe setup.

angle. For all measurements shown, the commanded path is represented by a dashed line, and the actual tool motion is shown as a (datapoint-to-datapoint) continuous line.

7.1. Corkscrew path

The results of the STLBB measurement of the corkscrew path are shown in Fig. 18. For this path, a counterclockwise half-circle was commanded in the X–Y plane, followed by a step in the −Z-direction. Next, the half-circle was completed and followed by another step in the −Z-direction, and so forth. In Fig. 19, the transition from the first half-circle to the first −Z motion in the corkscrew path is shown. The elliptical distortion of the half-circle in the X–Y plane is evident as well as undershoot in both the X- and Y-directions for the start of the −Z motion. The integral gain in the controller then begins to correct the steady-state error in the X- and Y-directions as the Z motion progresses.

7.2. Hemisphere path

The second CNC program roughly simulated a hemispherical cutting path. First, a small circle was executed in the X–Y plane. Next, a Y–Z linear interpolation was commanded, followed by a larger circle with the same center coordinates from this new starting point. The completion of this circle was followed by another linear motion, and so on. This path and a corresponding STLBB measurement is shown in Fig. 20. Fig. 21 shows the smallest circle in this path. It is immediately apparent that the circular path does not close and also exhibits an elliptical distortion due to the unequal X–Y controller gains. An X-axis reversal error can also be seen as the short Y-direction straight line motion during the circular interpolation.

7.3. Oblique circle

This path was executed in a plane oblique to each of the machine tool's coordinate axes. Fig. 22 shows the oblique circle path. Fig. 23 shows a selected portion of the projection of this path on the Y–Z plane. A modulation of the

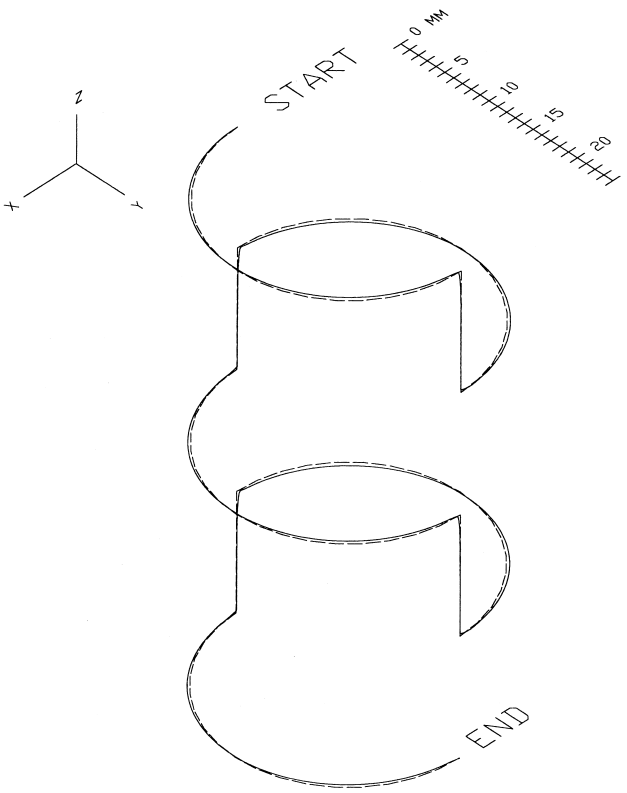

Fig. 18. Corkscrew path.

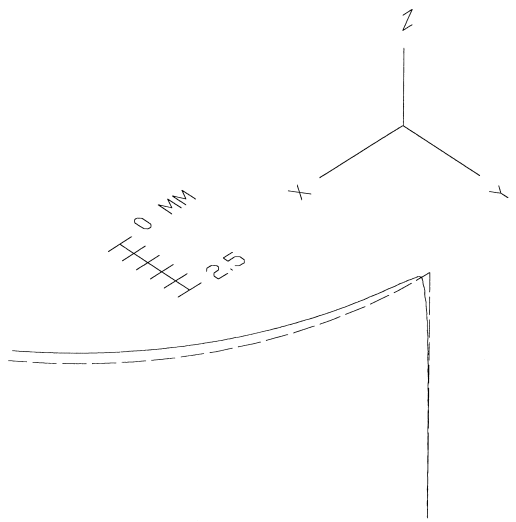

Fig. 19. Corkscrew path section.

Y-axis motion is apparent, followed by increasing error during the clockwise circular interpolation.

7.4. Oblique rectangle

Fig. 24 shows the commanded oblique rectangle contour and two different measurement results at feed rates of 889 and 1778 mm/min. Fig. 25 displays the section of the contour that includes the transition from −X, +Z linear interpolation to +X, +Y, +Z linear interpolation. The figure shows a steady-state error in the X–Z plane and undershoot errors at the interpolation direction transition.

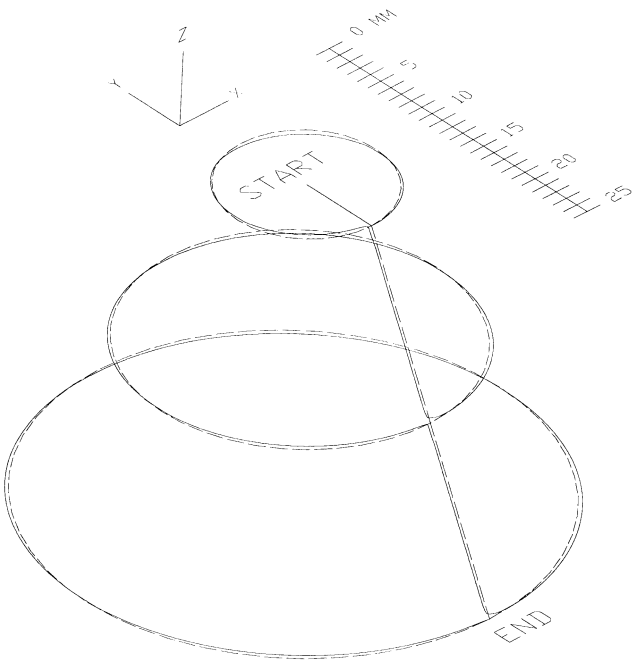

Fig. 20. Hemisphere path.

8. Evaluation of CNC contouring accuracy

Three applications of the STLBB evaluation of CNC contouring accuracy are now demonstrated. The first is the diagnosis of controller gain mismatches between all pairs of machine tool axes. The second use is to examine the source(s) of machine vibrations that modulate the spatial path of the tool. The third application involves the prediction of part dimensions from preprocess CNC path measurements.

9. Diagnosis of controller gain mismatch

The oblique rectangle path (Fig. 25) showed steady state following errors in all three planes. The individual projections of the selected cornering portion of the motion on the X–Y, X–Z, and Y–Z planes are given in Figs. 26 through 28. These plane views can be used to determine the gain relationships between the three axes of the available machine tool used in this study.

Using Fig. 26, the difference in gain between the X- and Y-axes (ΔK_{XY}) can be calculated. The expression for ΔK_{XY} is formulated in Eq. (1). To solve this equation, a value for either the X- or Y-axis gain must be known, because the measurement data only provide a difference between the X and Y positional lags (Δ_{XY}). The X-axis velocity lag ($e_{ss,x}$) was found by measuring the following error during a constant velocity move in the X-direction. These data were obtained by recording the commanded and actual encoder counts (using the machine tool's PMAC controller software), then determining the difference between the commanded and actual position under constant velocity motion. At a feed rate of 508 mm/min (20 ipm), this steady-state positional error was found to be 520 μm. The X-axis gain was then calculated according to Eq. (2).

$$\Delta K_{XY} = K_X - K_Y = K_X - \frac{F_Y}{e_{ss,Y}} = K_X - \frac{\frac{F_{\text{com}}}{\sqrt{2}}}{\frac{F_{\text{com}}}{\sqrt{2}}\frac{1}{K_X} + \Delta_{XY}} \tag{1}$$

$$K_X = \frac{F_X}{e_{ss,X}} = \frac{20\,\frac{25.4}{60}}{0.520} = 16.28\,\frac{1}{\text{sec}} \tag{2}$$

Referring again to Fig. 26, it is seen that the Y-axis lags 410 μm more than the X-axis during the constant velocity section of the 1778 mm/min +X, +Y motion. Substitution of this steady-state error difference, the experimental value for the X-axis gain, and the commanded path velocity (1778 mm/min or 70 ipm) into Eq. (1) yields a gain difference (ΔK_{XY}) of 3.93 s^{-1}. This value is positive, because the X gain is greater than the Y gain (i.e., the Y lag is greater than the X lag).

In Fig. 27, the X–Z gain relationship is found. As the motion progresses from the lower right-hand edge of the

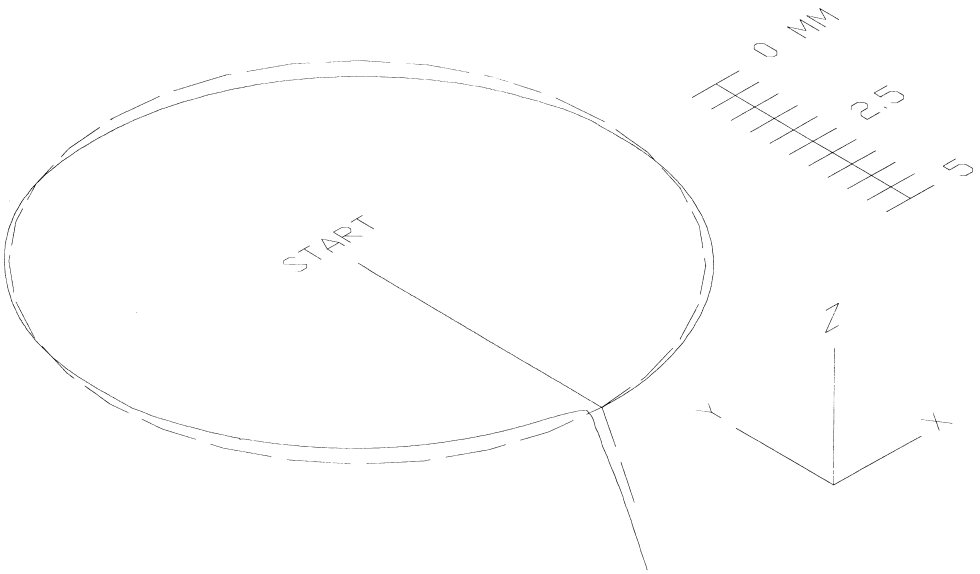

Fig. 21. Hemisphere path section.

figure to the upper right, the X motion lags more than the Z by 138 μm (at a commanded feed rate of 1778 mm/min). Therefore, the Z controller gain is larger than the X. Substitution into Eq. (3) yields a ΔK_{XZ} value of $-5.13\ s^{-1}$. Note that in Eq. (3), β_{XZ} is the angle between the X–Z plane and the commanded direction of motion.

$$\Delta K_{XZ} = K_X - K_Z = K_X - \frac{\frac{F}{\sqrt{2}}\cos\beta_{XZ}}{\frac{F}{\sqrt{2}}\frac{\cos\beta_{XZ}}{K_X} - \Delta_{XZ}} \quad (3)$$

Fig. 28 displays motion in the +Z-direction followed by a +Y, +Z linear interpolation. In this case, the Z controller gain is greater than the Y gain, because the Y lag is approximately 700 μm larger than the Z lag (at a feed rate of 1778 mm/min). The difference in gain, ΔK_{YZ}, may be calculated using Eq. (4). The calculated gain difference, $-8.84\ s^{-1}$, is negative, because the Y gain is smaller than the Z.

$$\Delta K_{YZ} = K_Y - K_Z = (K_X - \Delta K_{XY}) - (K_X - \Delta K_{XZ}) = -8.84 s^{-1} \quad (4)$$

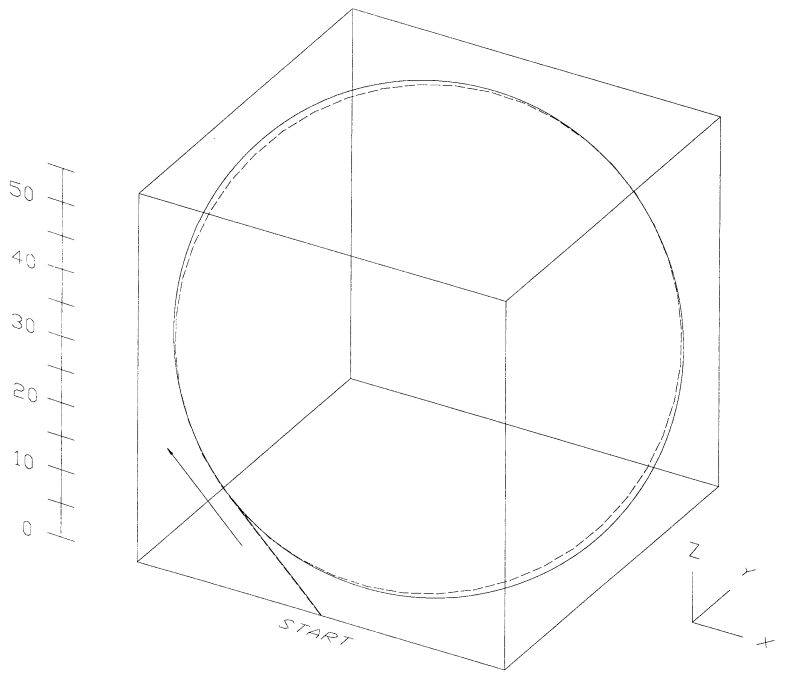

Fig. 22. Oblique circle path.

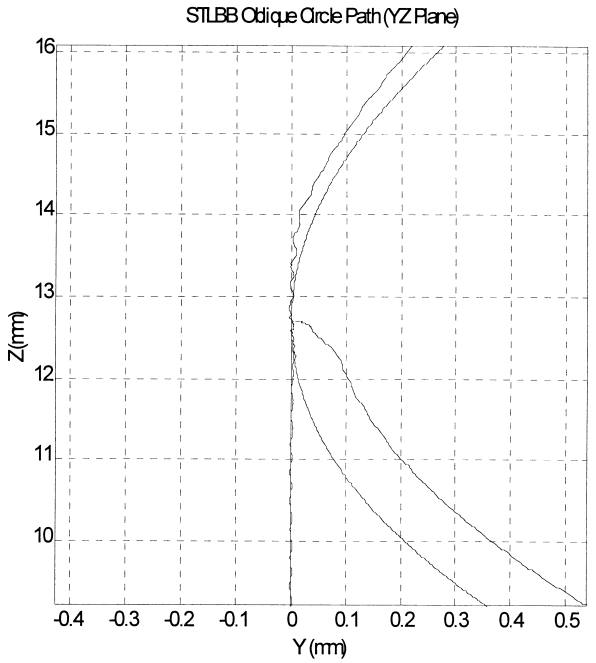

Fig. 23. Oblique circle section.

10. Path modulation by machine noise

As shown in Fig. 23, single axis motions on the machine tool used in this study were modulated by some high-frequency disturbance. To determine the source of this disturbance, the 3-D motions of the tool point were measured with the machine on (no commanded feed) and with the machine off (1 kHz sampling rate in both cases). The time-domain results of the "machine on" measurements are shown in Fig. 29 (with digital 4th order lowpass Butterworth filters applied). The frequency content of the "machine on"/"machine off" measurements is shown in Fig. 30 and 31. It can be seen in the measurements with the machine on that there is significant frequency content at 60, 120, and 180 Hz in the X-axis, 60 Hz in the Y-axis, and 60 and 120 Hz in the Z-axis. With the machine off, however, the frequency content drops to the noise floor threshold. The 60, 120, and 180 Hz frequency components in the machine noise were, therefore, attributed to the three-phase power of the axis motor amplifiers.

The single axis path modulation and corresponding frequency content is demonstrated in the Y and Z error mo-

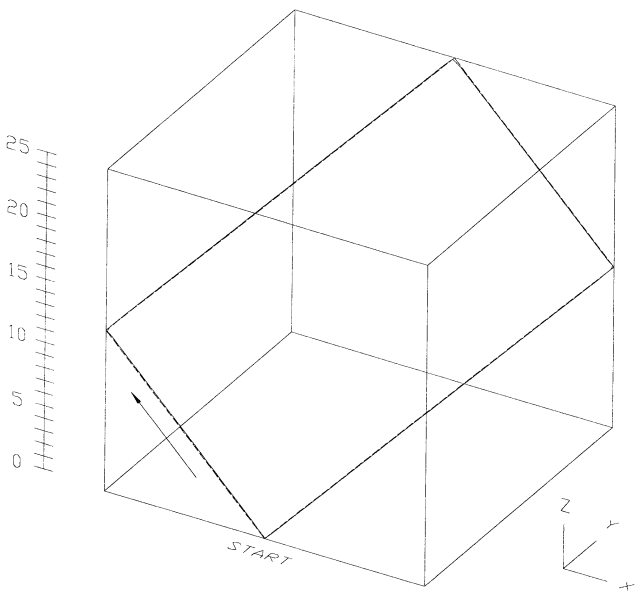

Fig. 24. Oblique rectangle path.

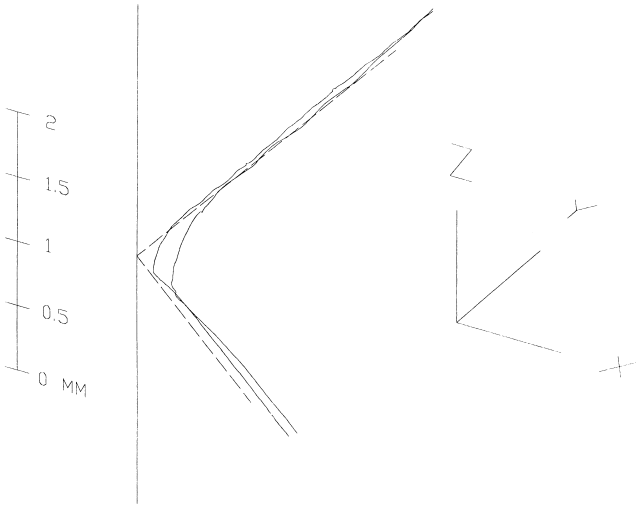

Fig. 25. Oblique rectangle path section.

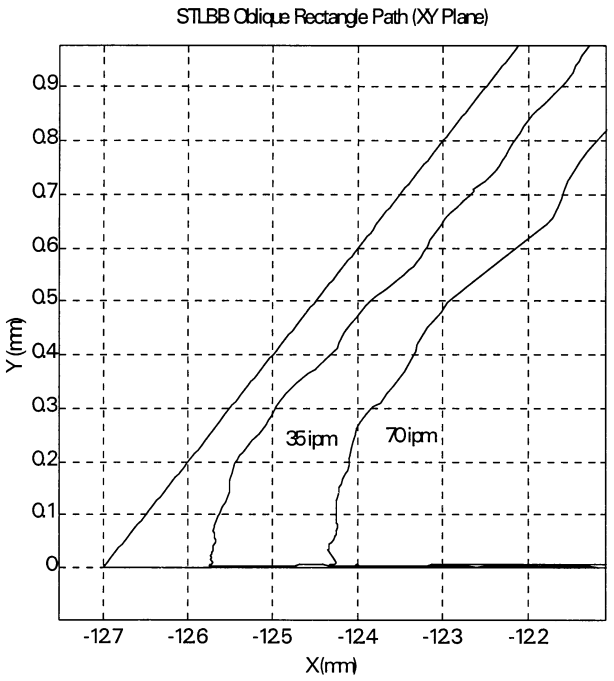

Fig. 26. Oblique rectangle path section (X–Y plane).

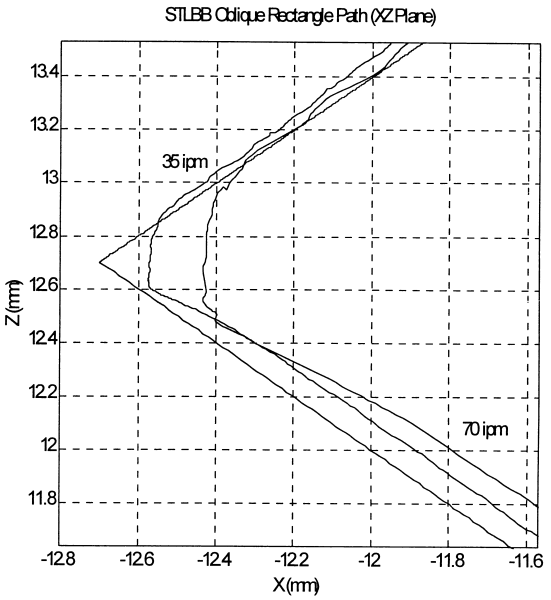

Fig. 27. Oblique rectangle path section (X–Z plane).

tions during a commanded X-axis travel shown in Figs. 32 and 33. It can be seen in Fig. 32 that the Y and Z motions (which are nominally zero) are modulated and cause a rapidly varying dynamic nonstraightness of motion. In Fig. 33, the expected frequency components are identified in each axis (60 Hz in Y and 60 and 120 in Z).

11. Comparison of measured trajectory to machined part dimensions

Perhaps the most traditional method for assessing the accuracy of CNC machine tools is to machine a test part and compare its actual dimensions to the dimensions commanded in the part program. See, for example, the Part Check (or Part Trace Test) in [11]. Because the purpose of the STLBB is to measure dynamic CNC tool paths, comparison of its measurements to machined part dimensions can also be used to evaluate the performance of the STLBB system. Although the STLBB system can measure 3-D dynamic contouring accuracy during the execution of arbitrary CNC contours, it cannot perform these measurements during the machining process (i.e., the CNC part path must be measured before cutting). Therefore, to verify the STLBB system by the manufacture of a test part, it is necessary to measure a given CNC contour, machine a part using the same part program, and then compare the results. However, the final part dimensions are also significantly affected by cutter/workpiece deflections attributable to the cutting forces [13], as well as by differences between the nominal and actual cutter diameter. Therefore, it is necessary to define the test part and measurement comparisons carefully, so as to eliminate these effects.

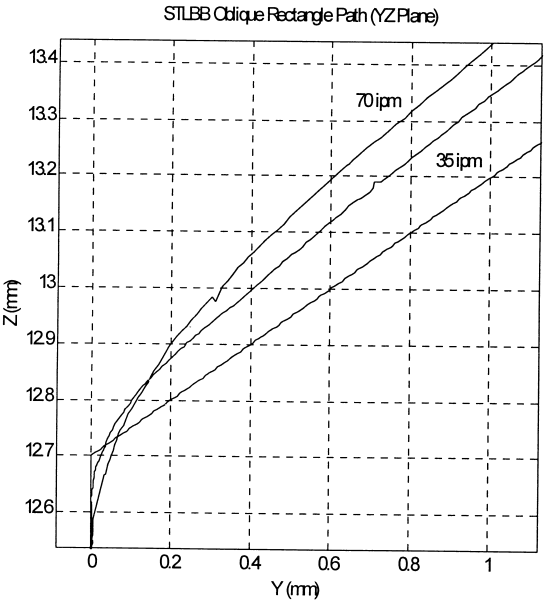

Fig. 28. Oblique rectangle path section (Y–Z plane).

To this end, we have chosen a diamond path (Fig. 34) to be executed in the X–Y plane of the machine at various feedrates. The X–Y gain mismatch observed during the angle path tests (Figs. 9 and 10) is expected to cause an offset, which is dependent on the commanded velocity, of the actual path from the commanded path. The total effect of the gain mismatch on the experimental diamond path is to lengthen the distance across one face (d_1, in Fig. 35) by twice the servo gain mismatch error and shorten the distance across the other (d_2 in Fig. 35), again by twice the gain mismatch error. The absolute magnitudes of d_1 and d_2 depend on the dynamic contouring errors, errors in the assumed cutter diameter, and also on deflections of the tool attributable to cutting forces. However, because the cutting force deflections and tool diameter errors affect all four sides of the diamond path equally, the difference between these dimensions, $\Delta d = d_1 - d_2$, is independent of these effects. Therefore, we use the metric, Δd, to compare the STLBB measurement results to the machined test part measurements. These results, as well as the experimental methodology, are presented in the following paragraphs.

11.1. STLBB results

By importing the STLBB measurements into AutoCAD® (version 14.0) via a script file, the distances (d_1 and d_2) were computed at nine different locations for each recorded path. Fig. 36 shows an example of the d_1 and d_2 experimental values for an 889 mm/min STLBB test. In Fig. 36, it can be seen that the previously discussed controller errors exert a sizable influence on the path straightness (i.e., large variation in d values) as the integral gain attempts to correct the steady-state error. Therefore, points very near the diamond edge were avoided. The final values for d_1 and d_2 were obtained by averaging the nine measurements across each face. The value for Δd was then calculated by subtracting the average d_2 value from the average d_1 value.

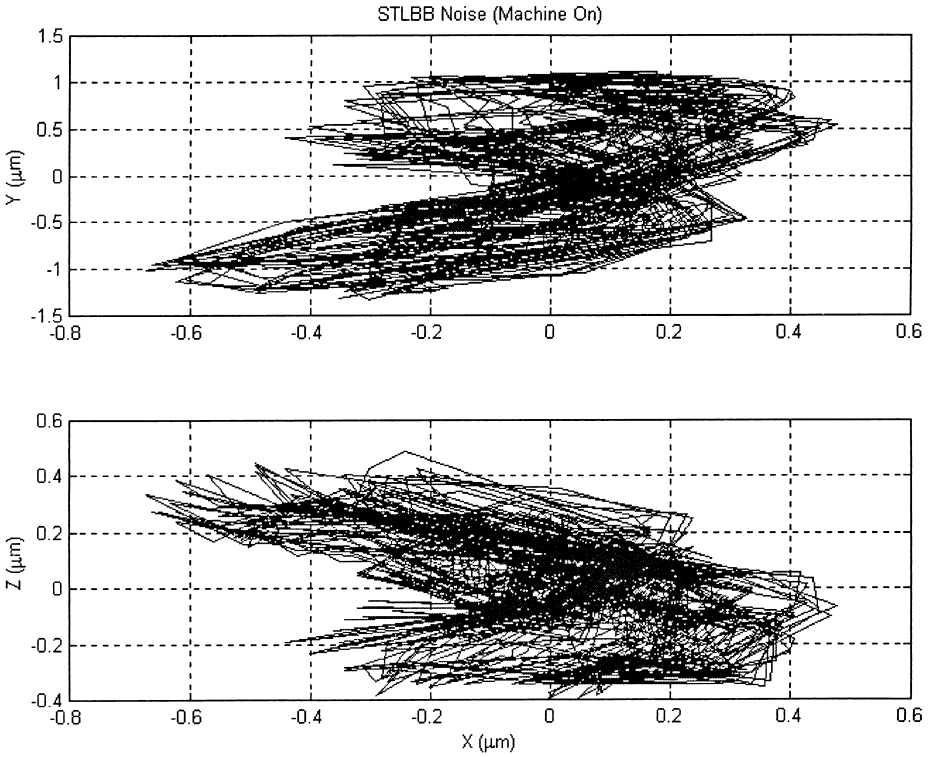

Fig. 29. Tool point motions (machine on).

This method was chosen, because it most closely corresponds to the CMM probing method used to measure the machined parts (i.e., 13 points were probed and a line best fit to the data in the CMM software). STLBB results for the two different feed rates are listed in Table 1. Also listed is the commanded value and the difference (Δd) between d_1 and d_2. It should be noted that these values reflect measurements of the actual tool path followed by the cutter.

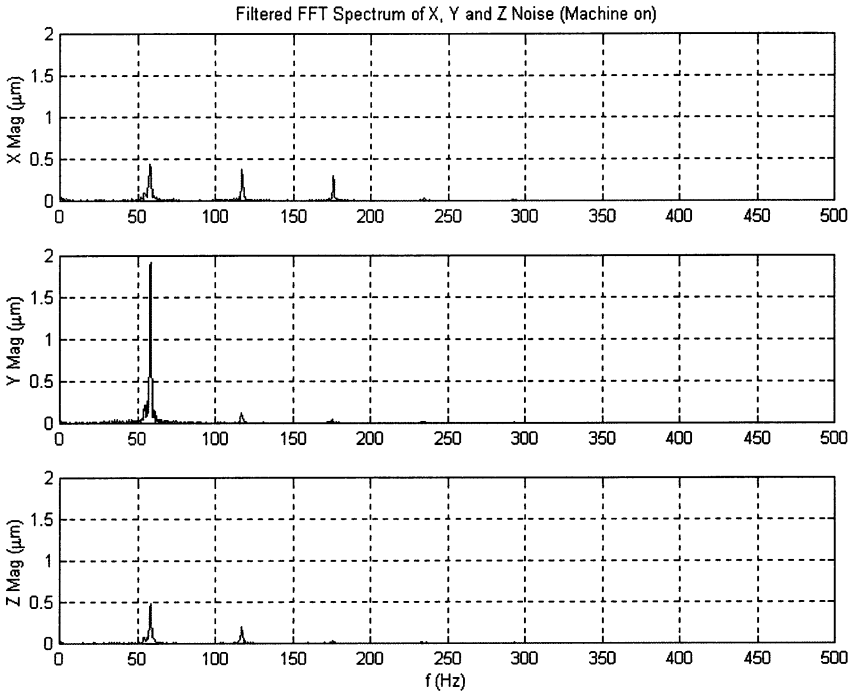

Fig. 30. Frequency content of X, Y and Z motions (machine on).

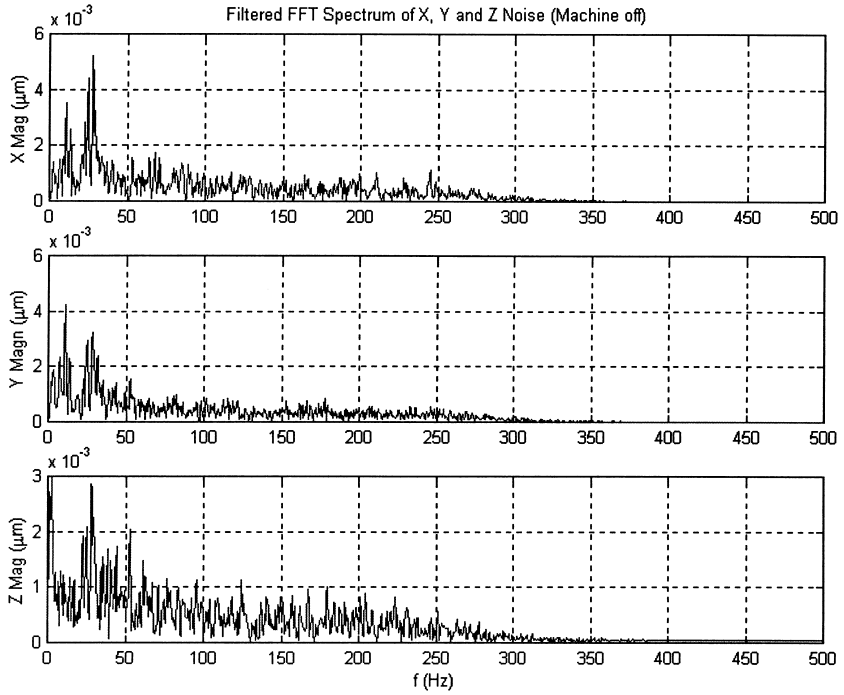

Fig. 31. Frequency content of X, Y and Z motions (machine off).

11.2. Diamond path machining results

The machining verification for the diamond path part was performed at the same two linear feed rates as the STLBB measurements, as well as the same commanded acceleration. The first test was executed under the following up-milling cutting conditions: 508 mm/min linear feed, 0.1 mm feed per tooth, 1337 rpm spindle speed, 1% radial immersion, and axial depth of cut equal to 0.254 mm. The low radial immersion was chosen to simulate a finishing

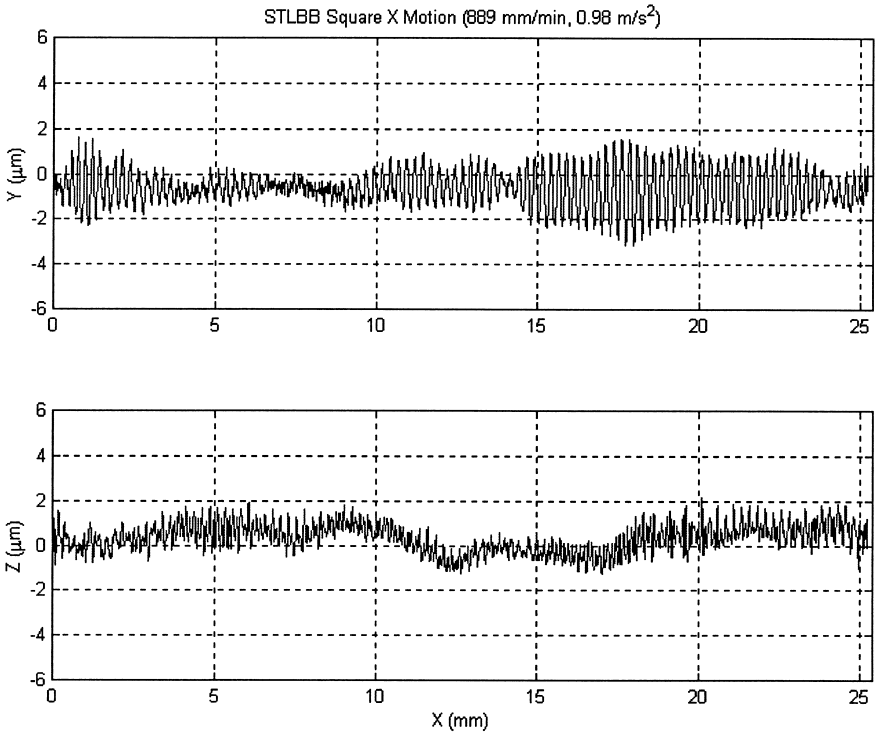

Fig. 32. Y and Z path modulation during X motion.

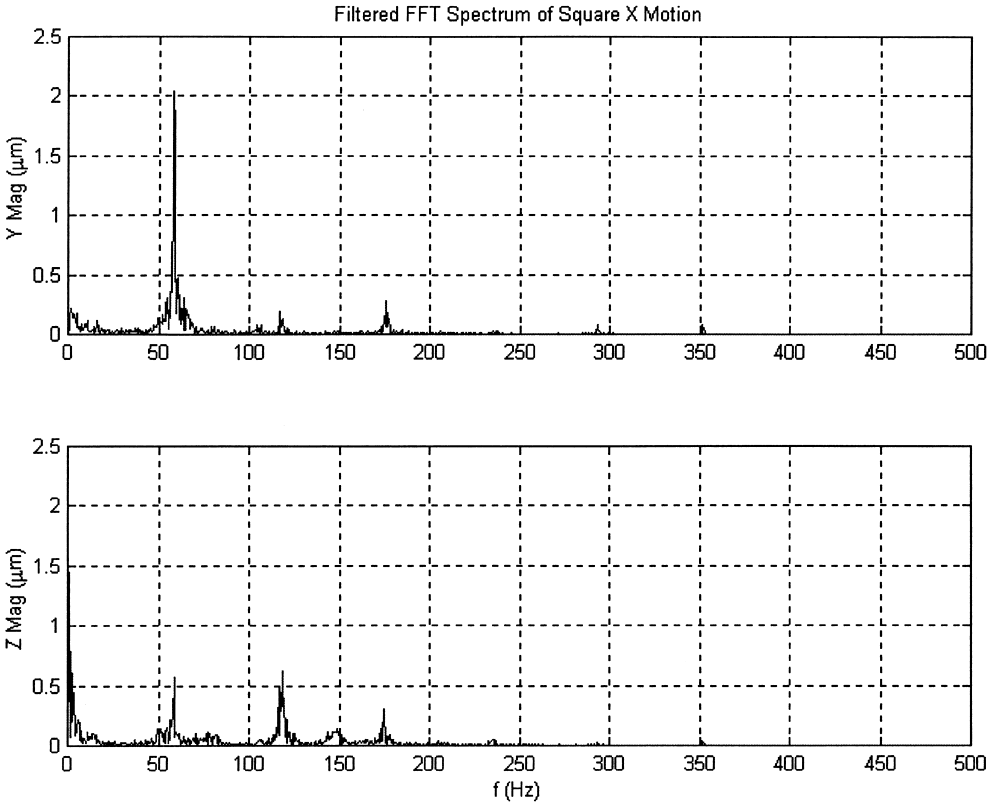

Fig. 33. Frequency content of Y and Z modulation (X motion).

operation and the low axial depth of cut avoided chatter, while minimizing any axial variations in surface location error attributable to the helical geometry of the cutter [13]. The second test was performed at 889 mm/min with a spindle speed of 2,339 rpm. All other cutting conditions were identical. The machining tests were performed at the same coordinates within the machine tool's work volume as the STLBB tests (to reduce the effect of the inherent position-dependent geometric inaccuracies of the machine) and the same approximate thermal state (the parts were machined from a cold thermal state). The same axis pretravels (+X, +Y) were also used to minimize reversal error contributions to part dimensional errors.

The cutting tool used for both tests was a nominal

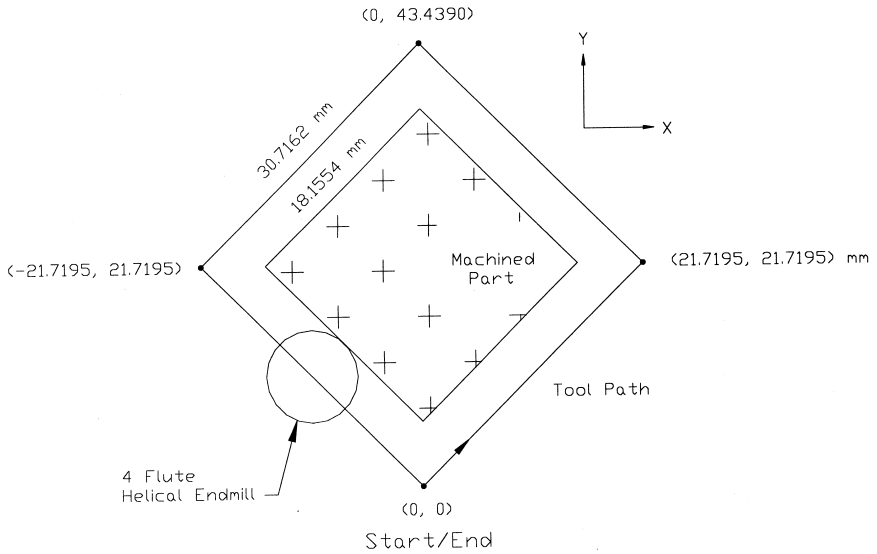

Fig. 34. Diamond path.

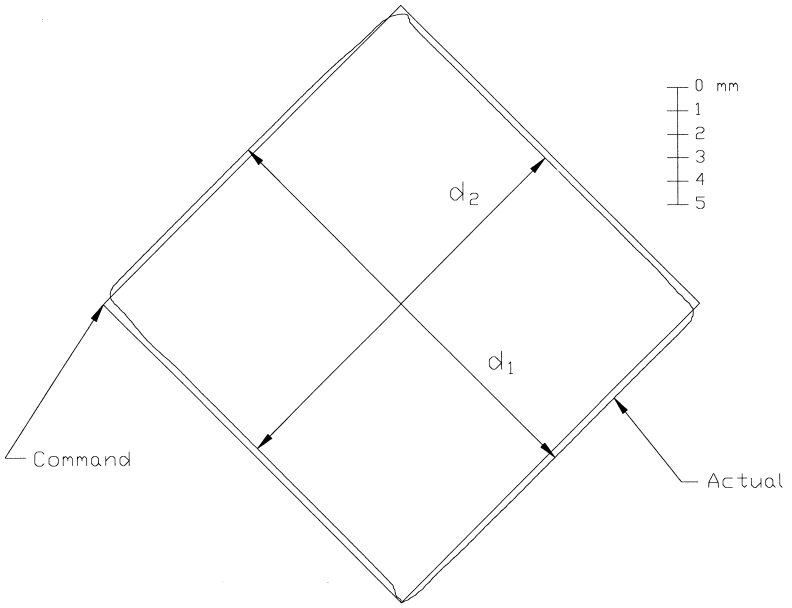

Fig. 35. STLBB diamond path (1778 mm/min).

12.7-mm diameter, 4-flute, high-speed steel (HSS) helical end mill extending 38 mm from the tool holder face. The frequency response function for the tool was obtained using an impact test. A curve fit to this data yielded modal values of 0.01 kg mass, 3.5e6 N/m stiffness, and a damping ratio of 0.03 for the most flexible mode at a natural frequency of 2950 Hz.

Once the diamond test parts were machined, they were allowed to soak overnight in a temperature-controlled environment (68 ± 0.2°F) and then measured on a Brown & Sharpe Micro Val PFx coordinate measuring machine. These measurements were completed under "Direct Computer Control" to improve the measurement accuracy. In this method, the part is first probed manually by the user (13 points were probed on each face of the diamond parts). The computer records the location in the CMM work volume of the measured features (four 2-D lines in this case) and then calculates the surface normal to each probed point. A corresponding part program is automatically written that includes the user-defined measurements and the appropriate approach directions. When this part program is executed, and the features are probed under computer control, the measurement accuracy (roughly ±1 μm for the portion of the work volume used in these measurements) is maximized because of the normal approach directions and constant (computer-controlled) approach speed. The measurement results for two machining verification parts are given in Table 2.

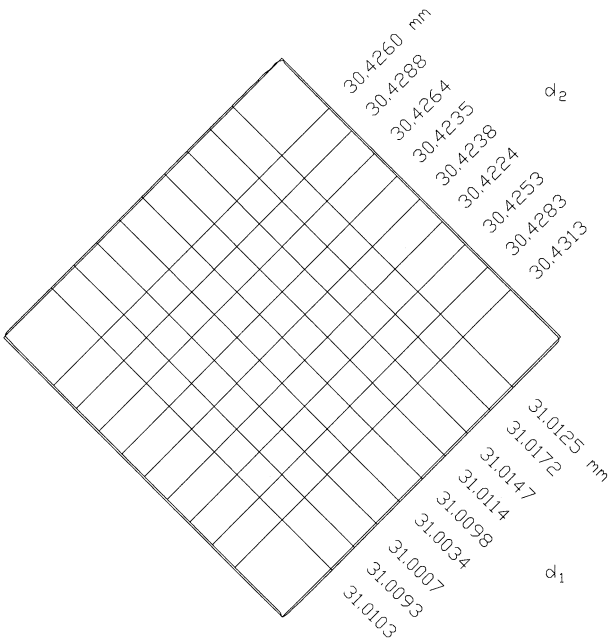

Fig. 36. Determination of Δd (889 mm/min).

Comparing these results with the STLBB dynamic contour measurements provides the final verification for the STLBB system. At 889 mm/min, the difference between the face dimensions of the diamond path, Δd, was measured as 0.5837 mm using the STLBB. The difference between the face dimensions for a machined part was then measured as 0.5839 mm using the CMM. These measurements agree to

Table 1
STLBB diamond path results

Feed rate	Commanded, d	Measured, d_1	Measured, d_2	Difference, Δd
508 mm/min	30.7162 mm	30.8891	30.5453	0.3438 mm
889 mm/min	30.7162	31.0099	30.4262	0.5837

Table 2
Machining verification results

Feed rate	Commanded, d	Measured, d_1	Measured, d_2	Difference, Δd
508 mm/min	18.1554 mm	18.3056	17.9712	0.3344 mm
889 mm/min	18.1554	18.4278	17.8439	0.5839

within 0.2 μm. The 508 mm/min tests provided a larger discrepancy of 9.4 μm. Table 3 shows a comparison of the machining and STLBB tests in tabular form.

To understand better the small measurement differences observed, several consecutive STLBB measurements and machining tests were completed to attempt to quantify the repeatability of Δd, the metric used to evaluate the STLBB performance in these tests. At 889 mm/min, the maximum difference between calculated Δd values for successive STLBB measurements was 3.5 μm. The maximum difference for Δd between sequential machined part measurements, again at a feed rate of 889 mm/min, was 5.2 μm. These repeatability errors are on the same order of magnitude as the differences seen between the STLBB and machined part measurements. This close agreement between the STLBB and machined part measurements further validates the STLBB system as a preprocess tool for CNC part program validation.

It should be noted that the diamond path used in this research represents a special case. Because the path is symmetric about both the X- and Y-axes, common path variations (such as surface location errors attributable to cutter deflections during machining, runout of the cutter, spindle error motions, or quasistatic spindle thermal growth errors) will not affect the metric (Δd) used to verify the STLBB system. Runout of the cutter teeth, for example, will affect both dimensions (d_1 and d_2) by the same amount and, therefore, have no effect on Δd. In addition, the path was kept small to minimize the introduction of the machine tool's parametric errors into the machined part geometry. In fact, this path was expressly chosen for the combination of the large X–Y gain mismatch errors and the absence of these other error sources.

In general, these special considerations cannot be met, and the cutting force and runout errors, as well as the machine tool's inherent parametric and thermal errors, can have a significant effect on the final dimensions of a machined part. For example, if an improper tool offset (tool diameter) is used in the CAD/CAM generation of complicated CNC part paths, significant part errors can be obtained as the cutter follows both inside and outside contours. Perhaps more insidious is the effect of forced vibrations during stable machining on the final part dimensions. In another publication [13], we have shown that machined part dimensions are dependent on the selected spindle speed, cutter dynamics, and chip load. Furthermore, significant variations in part dimensions may be obtained by relatively small variations of the spindle speed. These differences between the commanded and actual part dimensions attributable to cutting force effects have been termed *Surface Location Errors* [14]. To the uninformed observer, these surface location errors could be attributed to other common error sources (e.g., parametric, thermal, programming) and a significant amount of time wasted in attempting to diagnose and correct the problem.

Table 3
STLBB vs. machining verification results

Feed rate	Δd, STLBB	Δd, machining	Error
508 mm/min	0.3438 mm	0.3344	9.4 μm
889 mm/min	0.5837	0.5839	0.2 μm

12. Conclusions

We have developed an instrument capable of measuring arbitrary, dynamic CNC tool paths through 3-D space with micrometer-level accuracy. The measurement accuracy of the STLBB system was verified by comparison to a Heidenhain KGM 101 Grid Encoder using a number of different 2-D paths. The results of the two instruments were found to agree within the dynamic path repeatability of the machine tool used to produce the motions.

The STLBB measurement accuracy was also verified by measuring a diamond-shaped path and then machining a part using the same NC code. The dimensions of the machined part were measured on a CMM and compared to the STLBB results. The part shape and comparison metrics were specifically chosen to eliminate any contributions caused by imperfect knowledge of the cutter diameter, and any cutter deflections caused by the cutting forces. The STLBB path measurements were found to agree with the machined part measurements to within the repeatability of the machine tool.

Finally, the spatial dynamic path measurement capability of the STLBB was demonstrated for several 3-D paths. The utility of these measurements in identifying controller gain mismatch errors and servo switching frequency errors was shown.

Acknowledgment

This work was partially supported by the National Science Foundation under Grants DDM-935138 and GER-9354980 and the Department of Energy under the 1999 Integrated Manufacturing Predoctoral Fellowship.

References

[1] Donmez MA. A general methodology for machine tool accuracy enhancement: Theory application, and implementation. Ph.D. Dissertation, Purdue University, West Lafayette, IN, 1985.

[2] Srinivasa N. Modeling and prediction of thermally induced errors in machine tools using a laser ball bar and a neural network. Ph.D. Dissertation, University of Florida, Gainesville, FL, 1994.
[3] Chen JS, Ling C. Improving the machine accuracy through machine tool metrology and error correction. *Int J Manufact Technol* 1996; 11(3):198–205.
[4] Ziegert JC, Mize CD. Laser ball bar: A new instrument for machine tool metrology. *Prec Eng* 1994;16(4):259–67.
[5] Mize CD. Design and implementation of a laser ball bar based measurement technique for machine tool calibration. M.S. Thesis, University of Florida, Gainesville, FL, 1993.
[6] Schmitz T, Ziegert JC. A new sensor for the micrometre-level measurement of three-dimensional, dynamic contours. *Measure Sci Technol* 1999;10(2):51–62.
[7] Kulkarni RB. Design and evaluation of a technique to find the parametric errors of a numerically controlled machine tool using a laser ball bar. M.S. Thesis, University of Florida, Gainesville, FL, 1996.
[8] Mize CD, Ziegert JC, Pardue R, Zurcher N. Spatial measurement accuracy tests of the laser ball bar. Final Report for CRADA No. Y-1293-02244 between Martin Marietta Energy Systems and Tetra Precision, Inc., August 1994.
[9] Bryan JB. A simple method for testing measuring machines and machine tools Part 1: Principles and applications. *Prec Eng* 1982; 4(2):61–9.
[10] Bryan JB. A simple method for testing measuring machines and machine tools Part 2: Construction details. *Prec Eng* 1982;4(3):125–138.
[11] Bryan JB, Bowerbank JE, Holland ED, Mohl O. Updating tracer lathe machining operations. *ASTME* 1960;61(1):1–45.
[12] Bryan JB, Pearson JW. Machine tool metrology. Western Metal and Tool and ASTME Exposition and Golden Gate Conference, San Francisco, CA, September 24, 1968.
[13] Schmitz T, Ziegert JC. Examination of surface location error due to phasing of cutter vibrations. *Prec Eng* 1999;23(1):51–62.
[14] Tlusty J. EML 6934 Class Notes: Fundamentals of Production Engineering Part 2. University of Florida, Gainesville, FL, Fall Semester, 1994.